Reaction parameter study of the ^{51}V beam onto deformed targets: ^{51}V+^{159}Tb reaction

P. Brionnet[1,*], H. Haba[1], D. Kaji[1], S. Kimura[2], K. Morimoto[1], T. Niwase[3], S. Sakaguchi[3], and H. Sakai[1]

[1]RIKEN Nishina Center, 2-1 Hirosawa, Wako, Saitama 351-0106, Japan
[2]KEK Wako Nuclear Science Center, Wako, 351-0106, Sataima, Japan
[3]Department of Physics, Kyushu University, 744, Motooka, Nishi-ku, 819-0395, Fukuoka, Japan

Abstract. This study presents an experimental method to investigate the effects of side-collision configurations observed in the synthesis of superheavy nuclei, using lighter, deformed lanthanide targets. The research extends systematic studies of reactions involving beams heavier than ^{48}Ca on deformed targets. Measurements of both the entrance-channel barrier distribution and detailed excitation functions for the *x*n, p*x*n, and αxn channels, over a wide energy range, are provided for the ^{51}V+^{159}Tb system.

1 Introduction

The production of new elements and isotopes beyond nihonium (Z = 113) has, until now, been achieved using deformed actinide targets in combination with the doubly magic ^{48}Ca [1]. However, oganesson (Z = 118) was the last element accessible with this beam/target combination [2]. Indeed, beams like ^{50}Ti, ^{51}V, and ^{54}Cr are now necessary to access element Z = 119 and beyond. Such an attempt is currently underway at RIKEN, using the ^{51}V+ ^{248}Cm reaction. However, the recent synthesis of the ^{290}Lv isotope [3] has paved the way for the use of heavier beams, using the ^{50}Ti +^{244}Pu reaction.

Furthermore, reactions with deformed targets exhibit different behavior compared to reactions involving spherical Pb and Bi targets. Specifically, in reactions using deformed targets, the maximum production cross section is observed around the so-called side-collision configuration, rather than the tip-collision configuration. This side-collision effect has been previously studied in [4–6]. However, a systematic study of this effect in the superheavy nuclei region is challenging due to the very low production cross sections, ranging from femtobarns (fb) to picobarns (pb).

This study aimed to determine whether the side-collision effect could be observed and reproduced using lighter, deformed lanthanide targets. This work details the experimental method applied to the ^{51}V + ^{159}Tb system.

2 Experimental Setup

This experiment was conducted at RIKEN using the SRILAC accelerator [7], combined with the GARIS-III separator and detector station [7, 8]. The GARIS-III separator was set to maximize the transmission of the nuclei of interest (either target-like fragments or evaporation residues) to the focal plane detection system. The helium gas pressure in GARIS-III was optimized for each type of measurement: 0.9 Torr during the barrier distribution measurements, and 0.55 Torr for the excitation function measurements.

The focal plane detection system consists of two sets of detectors. First, two high-performance time-of-flight detectors are positioned at the exit of the separator, enabling the detection and identification of incoming ions based on their masses. Next, a silicon box is placed at the focal plane of the separator for the implantation and detection of the subsequent decay of the nuclei of interest. A detailed description and characteristics of this experimental setup are provided in [7].

3 Experimental Method

For the first time, a direct measurement of both the quasi-elastic barrier distribution and detailed fusion-evaporation excitation functions across a wide range of exit channels (*xn*, *pxn*, αxn, etc.) was performed in a single experimental campaign. This combined measurement enables a direct comparison between the two, providing insights into the entrance-channel versus side-collision effect [4, 5] on production rates.

This proceeding primarily focuses on the experimental method used in the study of the ^{51}V + ^{159}Tb system, with the complete analysis presented by P. Brionnet *et al.* [9].

3.1 Barrier distribution

The quasi-elastic barrier distribution measurement was conducted similarly to the methods described in [4, 5]. The GARIS-III separator was configured to transport

*e-mail: pierre.brionnet@riken.jp

backscattered target-like nuclei at $\theta_{\rm lab} = 0°$. Detection and identification of these target-like nuclei at the focal plane were achieved by correlating the timing information from the TOF detector with the implantation energy in the DSSD. Identification and rejection of background events were based on the mass of the incoming ions.

Throughout the experiment, close monitoring and correction of the transmission of events of interest were necessary, as the implantation profile of the target-like events in the detection system closely matched its dimensions, specifically the entrance window of the TOF detector and the X-axis size of the DSSD. This monitoring and correction were performed by measuring the transmission dependence relative to the center of the implantation distribution at different beam energies. The quasi-elastic barrier distribution, $D(E_{\rm c.m.})$, is defined by the following equation:

$$D(E_{\rm c.m.}) = -\frac{dR(E_{\rm c.m.})}{dE_{\rm c.m.}} \equiv -\frac{d}{dE_{\rm c.m.}}\left(\frac{d\sigma_{\rm QE}}{d\sigma_{\rm Ruth}}\right). \quad (1)$$

$R(E_{\rm c.m.}) \equiv \frac{d\sigma_{\rm QE}}{d\sigma_{\rm Ruth}}$ is referred to as the reflection probability and represents the ratio of the quasi-elastic (QE) backscattering cross section to the Rutherford scattering cross section at a fixed angle at the target position. Experimentally, $R(E_{\rm c.m.})$ is extracted by directly taking the ratio of the number of ^{51}V ions detected at the target position, $N_{\rm Ruth}[^{51}{\rm V}]$, to the number of recoiled QE backscattered ^{159}Tb-like ions measured at the focal plane, $N_{\rm QE}[^{159}{\rm Tb}]$:

$$R(E_{\rm c.m.}) \equiv C \times \frac{N_{\rm QE}[^{159}{\rm Tb}]}{N_{\rm Ruth}[^{51}{\rm V}]}, \quad (2)$$

where C is the normalization coefficient of the reflection probability. The barrier distribution is then derived from the $R(E_{\rm c.m.})$ distribution using:

$$D(E_i) = -\frac{R(E_{i+1}) - R(E_{i-1})}{E_{i+1} - E_{i-1}}. \quad (3)$$

The entrance-channel barrier value, B_0, is defined as the energy where $R(B_0) = 0.5$. This value is extracted through linear extrapolation of the $R(E_{\rm c.m.})$ distribution around the 0.5 mark. The side-collision barrier energy cannot be directly obtained from the measured distribution; instead, it is extracted using coupled-channel calculations with the CCFULL code [10]. The parameters of the code are optimized to reproduce both the experimental $R(E_{\rm c.m.})$ and $D(E_{\rm c.m.})$ distributions.

3.2 Excitation function measurement

For the excitation function measurement, a wide variety of exit channels (xn, pxn, αxn, αpxn, ...) were transported by the GARIS-III separator simultaneously. Consequently, the transmission of GARIS-III for each exit channel needed to be corrected for the cross-section estimate.

At the focal plane position, this correction was performed by estimating the magnetic rigidity, Bρ, of each exit channel using the formula from [11]. Then, using one channel with an implantation distribution centered in the DSSD as a reference, the transmission of the other transmitted nuclei was corrected based on their deviation from the reference, utilizing the known dispersion of GARIS-III [8]. At the target position, the transmission depends on the solid angle of emission after the target. Monte Carlo simulations were developed to estimate this solid angle for each channel and compare it to the known angular acceptance of GARIS-III [8].

The yields of the individual exit channels were estimated using the total α-spectrum without any time selection. Each spectrum was accumulated over 24 hours, including one hour of beam-off between each measurement to reduce cross-contamination from long-lived isotopes. For each exit channel, all nuclei produced in the decay chain were listed along with their reported decay characteristics and uncertainties: decay energy and branching ratio. The total theoretical α-spectrum was then used to fit the measured α-spectrum and extract the production yield of each exit channel. The number of channels considered at each beam energy was also adjusted for stability, meaning not all channels were taken into account at each beam energy.

4 Results overview

The identification of the target-like nuclei for the barrier distribution measurement is presented in Fig.1.

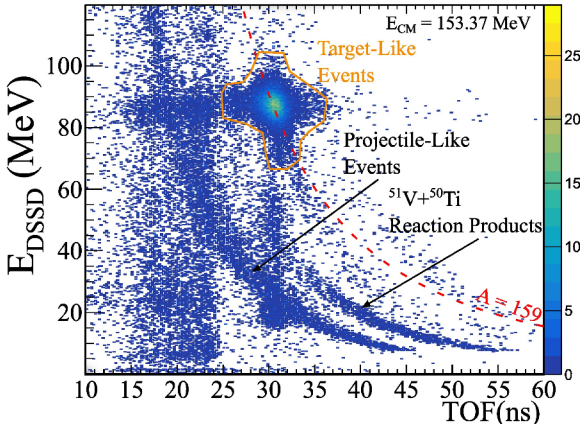

Figure 1. Identification of the ions exiting the separator during the quasi-elastic barrier measurement at $E_{c.m.}$=153.37 MeV using the time-of-flight/energy correlation: the orange line corresponds to the target-like nuclei, the dashed red line is the mass A=159, and the black arrows point to the main background components.

Based on the detected target-like nuclei and using Eqs. 2 and 3, we can obtain the reflection probability distribution $R(E_{\rm c.m.})$ (Fig.2(a)) and the quasi-elastic barrier distribution $D(E_{\rm c.m.})$ (Fig.2(b)). The dashed lines in Fig.2 correspond to the CCFULL calculations run under different sets of parameters: fully optimized, with and without the target deformation parameter, ... The dotted line represents the side-collision barrier extracted from these calculations. From these distributions and calculations, the entrance barrier height B_0 is 164.12±0.42 MeV, while the side collision barrier height $B_{\rm side}$ is approximately 171.5 ± 0.5 MeV.

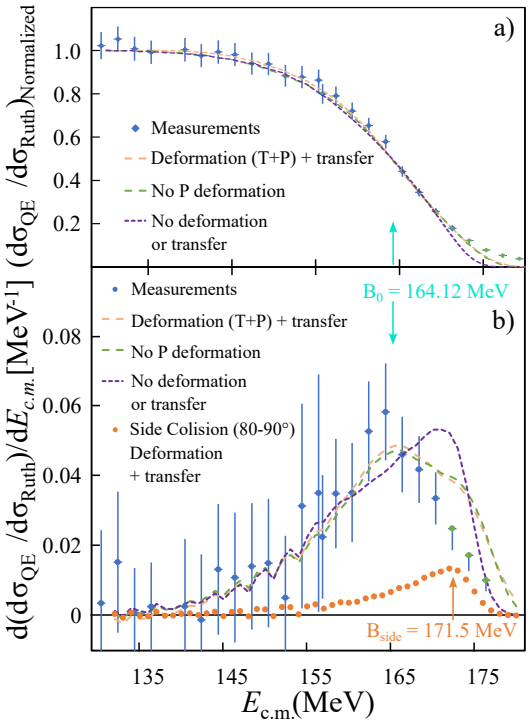

Figure 2. Measured reflection probability $R(E_{\mathrm{c.m.}})$ (a) and the QE barrier distribution $D(E_{\mathrm{c.m.}})$ (b) compared to the CCFULL calculations [10] based on different assumptions. The dotted line is the side-collision barrier extracted from such calculation.

Figure 3 plots the fusion-evaporation cross section for the ^{51}V+^{159}Tb→^{210}Ra* reaction extracted from the measured spectrum.

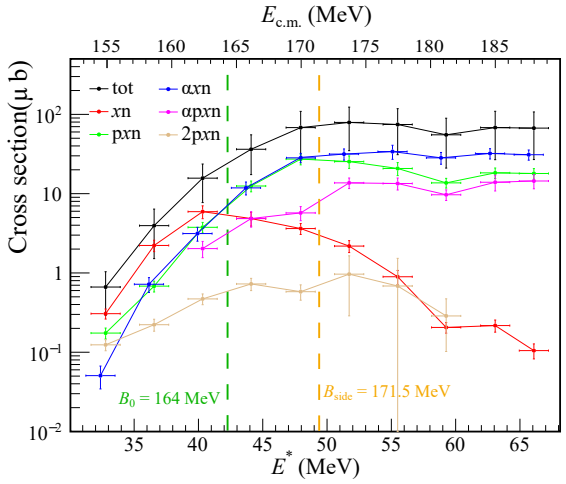

Figure 3. Measured total cross sections: total evaporation-residue cross section in black, sum of the xn, pxn, αxn, αpxn and 2pxn reaction channels in red, green, blue, pink, and light brown, respectively. The vertical dashed lines represent the values of B_0 (green) and B_{side} (orange).

Interestingly, for this reaction, we observed an enhancement of the charged particle cross section, with the maximum cross section being $\approx 41.7 \pm 5$ µb for the α3n reaction channel at $E_{\mathrm{c.m.}} = 177.7 \pm 1.5$ MeV. The maximum of the xn channels is the 3n channel, with a cross section of only 4.7 ± 1.5 µb at $E_{\mathrm{c.m.}} = 162.5 \pm 1.5$ MeV. This measurement contrasts with other reactions performed with ^{48}Ca/^{50}Ti on the same target [13, 14], where this enhancement was not observed. These behaviors and values are well reproduced by the statistical model calculation [12].

References

[1] Y., Oganessian, Utyonkov, Rep. Prog. Phys **78**, 036301 (2015). 10.1088/0034-4885/78/3/036301
[2] J., Roberto et. al.,Nuclear Physics A **944** 99 (2015). 10.1016/j.nuclphysa.2015.06.009
[3] J. Gates et. al., ArXiv Preprint ArXiv:2407.16079 (2024). 10.48550/arXiv.2407.16079
[4] M., Tanaka et. al.,J. Phys. Soc. Jpn.. **91**, 084201 (2022). /10.7566/JPSJ.91.084201
[5] T. Tanaka et. al., Phys. Rev. Lett. **124**, 052502 (2020). 10.1103/PhysRevLett.124.052502
[6] D. Hinde et. al., Phys. Rev. Lett. **74**, 1295 (1995). 10.1103/PhysRevLett.74.1295
[7] H. Sakai et al., Eur. Phys. J. A **58**, 238 (2022). 10.1140/epja/s10050-022-00888-3
[8] D. Kaji et. al., Nucl. Instrum. Methods Phys. Res. B **317**, 311 (2013). 10.1016/j.nimb.2013.05.085
[9] P. Brionnet et. al., Phys. Rev. C **110**, 064601 (2024). 10.1103/PhysRevC.110.064601
[10] K. Hagino et al., Comp. Phys. Comm. **123**, 143 (1999). 10.1016/S0010-4655(99)00243-X
[11] K. Gregorich et. al., Phys. Rev. C **72**, 014605 (2005). 10.1103/PhysRevC.72.014605
[12] K. Siwek-Wilczyńska, J. Wilczyńska, Phys. Rev. C **69**, 024611 (2004). 10.1103/PhysRevC.69.024611
[13] D. Mayorov et. al., Phys. Rev. C **90**, 024602 (2014). 10.1103/PhysRevC.90.024602
[14] D. Mayorov et. al., Phys. Rev. C **92**, 054601 (2015). 10.1103/PhysRevC.92.054601